RSC Advances

This is an *Accepted Manuscript*, which has been through the Royal Society of Chemistry peer review process and has been accepted for publication.

Accepted Manuscripts are published online shortly after acceptance, before technical editing, formatting and proof reading. Using this free service, authors can make their results available to the community, in citable form, before we publish the edited article. This *Accepted Manuscript* will be replaced by the edited, formatted and paginated article as soon as this is available.

You can find more information about *Accepted Manuscripts* in the Information for Authors.

Please note that technical editing may introduce minor changes to the text and/or graphics, which may alter content. The journal's standard Terms & Conditions and the Ethical guidelines still apply. In no event shall the Royal Society of Chemistry be held responsible for any errors or omissions in this *Accepted Manuscript* or any consequences arising from the use of any information it contains.

ROYAL SOCIETY OF CHEMISTRY

www.rsc.org/advances

Preparation of structurally colored films assembled by Polystyrene@Silica, air@Silica and air@Carbon@Silica core-shell nanoparticles with enhanced color visibility

Fen Wang, Xin Zhang, Jianfeng Zhu and Lin Ying

School of Materials Science and Engineering, Shaanxi University of Science and Technology, Xi'an 710021, China

Abstract

PS (Polystyrene)@SiO_2 (Silica) core-shell nanospheres were synthesized through a surfactant-free method followed with a modified Stöber method in this work. Hollow SiO_2 was abtained by calcining the PS@SiO_2 core-shell nanoparticles (NPs) at 500 ^oC in air and air@C(Carbon)@SiO_2 was prepared by calcining PS@SiO_2 in argon. SEM, TEM were used to confirm the formation of homogeneous SiO_2 shell on the negatively charged PS beads. EDS element mapping was utilized to confirm the existence and homogeneity of C layer in the air@C@SiO_2 nanospheres. After calcination, C was partly remained inside the SiO_2 shell and function as absorb materials. The advantages of using negatively charged PS beads to prepare PS@SiO_2 core-shell NPs and calcination PS@SiO_2 in argon to prepare hollow SiO_2 are: (1) the lower cost compared with the positively charged PS beads, since the negatively charged PS beads could be obtained with using cheap anionic initiators (such as KPS); (2) The color saturation of the photonic crystals (PCs) composed by hollow SiO_2 is significantly enhanced without disturbing PCs arrays when the calcination process is carried out in argon. Hollow SiO_2 PCs with enhanced color saturation will enrich the application[1] of core-shell structures in many fields such as bionic colors, paintings,

[1] Corresponding author: Tel.: +8615114805183; fax: +8602986168688.

RSC Advances Accepted Manuscript

cosmetics, and photonic papers.

Keywords: Hollow SiO_2, air@C@SiO_2, calcination, argon protection, enhanced color saturation.

1. Introduction

Photonic crystals (PCs) with the presence of a photonic stop band have many potential technological applications, such as optical communications, photonic computing, switching, sensing, lasing, and solar cells. [1-9]

SiO_2 as a primary component of soil has been widely used to fabricate PCs. Moreover, toxicity of silica particles that are greater than 300 nm in diameter had not been found in vivo. And sub-micrometer sized SiO_2 NPs become one of the best candidates for fabricating the environmental friendly materials. [10-11]

Brilliant PCs structural color is arising from interference, diffraction, or scattering in periodic arrays according to the Bragg Equation in visible region. [12-14] Recently, PCs assembled by hollow spheres with novel geometry structures have received considerable attentions. And PCs of hollow spheres were expected to be used as support to synthesize materials with full photonic band gaps. [15-20] Core-shell NPs is one of the new building blocks for fabricating PCs with photonic properties vary from those single materials. [21] To obtain hybrid, multi-functional colloidal NPs, core-shell NPs provide a simple way to incorporate different materials into the same structure. [22-25] As a widely used coating material, SiO_2 has many advantages: First, SiO_2 is hydrophilic and negatively charged, which can prevent the aggregation of the colloidal particles; second, hollow SiO_2 could be easily obtained by removing the core via calcination or etching. [26-32]

Negatively charged Polystyrene (PS) beads with uniform spherical shape become one of the

E-mail address: wangf@sust.edu.cn (F. Wang)

RSC Advances Accepted Manuscript

widely used template materials. Moreover, it could be obtained by using cheap anionic initiators (e.g., KPS) and the cost of which is lower compared to the positively charged PS beads.[26-27, 33] Stöber method could be employed to fabricate SiO_2 coating on PS, if one handles the surface charge properly. [34-35, 37-40] In general, negatively charged PS beads were not suitable to be used as core materials for the deposition of SiO_2 on them directly, due to the existence of strong electrostatic repulsive force. [35, 36] And SiO_2 particles were tend to independently existed in the ethanol solution instead of depositing on the surface of negatively charged PS beads. However, Jiang et al. [36] found that SiO_2 shell could be coated on the surface of negatively charged PS beads with the help of a nonionic surfactant (such as PVP), but this method involves several steps. Most recently, Deng et al. [35] reported homogeneous PS@Vinyl-SiO_2 core–shell particles by using Vinyl silane three oxygen radicals (VTMS) as a precursor of SiO_2, and high yield of SiO_2 coating on negatively charged PS beads was obtained in this way. However, expensive raw material was not suitable for mass production. Previously, Xia and co-workers [34] also reported a simple one-step method to prepare the PCs of PS-core SiO_2-shell spheres by selecting the PS spheres terminated in the -NH_2 group. In addition, color saturation is also very important for PCs. But PCs assembled by hollow spheres usually have a low color visibility since there is only a thin layer of high refractive index material and induced a small effective modulation of the refractive index. [15]

Black materials with high absorption in visible region could be used to enhance the color saturation and the color saturation could be enhanced significantly by mixing black materials of several nanometers (such as acetylene black and Fe_3O_4) into colloidal systems. [41-45] But this method is not suitable for preparing PCs since they were tended to cause defects and break down the long range order inevitably.

RSC Advances Accepted Manuscript

Herein, homogeneous PS@SiO_2 core-shell NPs were prepared by a simple surfactant-free method and a modified Stöber method. Air@SiO_2 and Air@C@SiO_2 were obtained by calcining the PS@SiO_2 at 500 ^oC in air and argon, respectively. The advantages of using negatively charged PS beads to prepare PS@SiO_2 core-shell NPs and calcination PS@SiO_2 in argon to prepare hollow SiO_2 are: (1) the lower cost of negatively charged PS beads compared with the positively charged PS beads, since the negatively charged PS beads could be obtained by using cheap anionic initiators (such as KPS); (2) The color saturation of PCs assembled by hollow SiO_2 is significantly enhanced without disturbing PCs arrays when calcination process is carried out in argon. PCs of air@C@SiO_2 with enhanced color saturation will enrich the application of core-shell structure in many fields such as bionic colors, paintings, cosmetics, and photonic papers.

2. Experimental Sections

2.1. Chemicals and Materials

Styrene (St), sodium hydroxide (NaOH), potassium persulfate (KPS), Tetraethoxysilane (TEOS), ethanol, and ammonia (28%) were purchased from Sinopharm Chemical Reagent Co., Ltd of China. Concentrated sulfuric acid (H_2SO_4) (96%), methacrylic acid (MAA) and hydrogen peroxide (H_2O_2) (30%) were all purchased from Tianli Chemical Reagent Co., Ltd., China. St was extracted by washing with aqueous NaOH (5 wt %) for three times, followed by deionized water for six times, respectively. Other reagents of analytically grade were directly utilized without further purification. Deionized water (18.2 MΩ. cm resistivity) was used in all experiments. The glass substrate was treated in a mixture containing concentrated 98% H_2SO_4 and 30% H_2O_2 with a volume ratio of H_2SO_4/H_2O_2 = 3:1 v/v) at 60 ^oC for 2 h before use.

2.2. Synthesis of PS NPs.

RSC Advances Accepted Manuscript

Emulsifier-free emulsion polymerization method was used to synthesize PS NPs. In a typically process, polytetrafluoroethylene stirring rod was fixed on a 250 ml three-neck round-bottomed flask in an oil bath. 100.0 ml deionized water, 6.0-8.0 ml St and 1ml of MAA were added into the flask at room temperature and slowly heated to 75.0 ºC under a speed of nearly 300 rpm. Then, 5.0 ml of deionized water containing 0.15 g KPS was poured into the flask as quickly as possible. Experiment was carried out under nitrogen atmosphere and kept at the constant temperature for 8 h. Finally, the PS suspension was washed with ethanol for three times and stored in ethanol for use.

2.3. Preparation of monodisperse PS@SiO_2 spheres.

Generally, PS beads terminated in -SO_3H or -COOH group were considered to be negatively charged. And it is hardly to develop SiO_2 coating directly on PS nanospheres with a negative charge on surface. However, PS beads terminated in the -NH_2 group were considered to be slightly positively charged or essentially neutral, which could be easily coated with uniform shells of amorphous silica by controlling the hydrolysis and condensation of TEOS precursor.

In this study, SiO_2 shell was prepared by a modified Stöber procedure involves the slow hydrolysis and condensation of TEOS. In a typical synthesis, 0.03 g PS nanospheres completely dispersed in a mixture of 2 mL deionized water and 35 mL ethanol by ultrasonic. To make PS nanospheres terminated in -NH_2 group, 0.5 mL ammonia was added into the reactor under constant stirring for 60 min. Then, various amounts of TEOS (as specified in each figure caption) were poured into the flask as quickly as possible. The hydrolysis reaction was allowed to proceed at room temperature for 8 h under constant magnetic stirring. Finally, the colloidal dispersions were collected by centrifugation. Due to the negative charges on the surface of silica shells, the core-shell particles

RSC Advances Accepted Manuscript

could form stable suspensions in aqueous mediums without adding any surfactant.

2.4. Crystallization of the Core-Shell nanospheres.

3D PCs of PS and PS@SiO_2 spheres were fabricated by using a simple vertical deposition method.[15] In a typical process: first, about 0.01-0.02g dried PS powder or 0.02-0.04g PS@SiO_2 powder were dispersed in 10 ML of ethanol by ultrasonic for 30 min at ambient temperature. Then those dispersions were poured into a 25 ML beaker and glass substrates were carefully placed into the beaker. The whole process was carried out at 40 ^{o}C for PS and 50 ^{o}C for PS@SiO_2.

2.5. Fabrication of silica shell PCs.

PCs of hollow SiO_2 were acquired by calcining PS@SiO_2 at 500 ^{o}C. The calcination process in detail was described as follow: the PCs samples were calcined at 500 ^{o}C in a rate of 3 ^{o}C /min and kept at 500 ^{o}C for 2 h in argon protection. For comparison, we also calcined the samples in air. Finally, the samples were natural cooling in the furnace.

2.6. Characterization.

Transmission electron microscope (TEM) (FEI Tecnai G2 F20 S-TWIN) was used for observing the morphology and measuring the geometric parameters of the particles. The samples were prepared by dipping a carbon coated copper grid into a diluted ethanol solution of particles, taking out the copper grid, and evaporating the ethanol solvent.

The morphology of colloidal crystal films was observed by using scanning electron microscopy (SEM) (Hitachi S4800). A thin Au layer (10 nm) was sputtered on the film before observing. The reflection spectra of the colloidal crystals were recorded by using a Cary 5000 UV−vis-NIR spectrometer (Agilen).

The optical photographs and microscopy images of the fabricated APSs were taken by an optical

RSC Advances Accepted Manuscript

microscope (Leica DM2500 M) connected with a CCD camera.

The diameter of PS spheres, PS@SiO_2 spheres and hollow silica spheres were determined by a statistical method. For example, the mean diameter of spheres was obtained by statistical diameter about 30 spheres from the SEM images. The inner diameter of hollow silica spheres and the thickness of silica shells were also determined by the statistical method from TEM images.

^{1}H NMR spectra were taken on a Bruker AV400 nuclear magnetic resonance spectrometer (NMR) with a proton frequency of 300 MHz and the solvent was DMSO-$_{d6}$. FTIR spectra were recorded with Agilent FTIR8400S Fourier Transform Infrared spectrometer in KBr pellets between 6000 and 20 cm^{-1} in air.

3. Results and discussion.

3.1 Characterization of PS@SiO_2 spheres and photonic crystal films

In this study, PS templates of 180±5 nm, 200±5 nm, 240±5 nm, and 290±5 nm in size with a low polydispersity have been synthesized in advance. SEM images in Fig. S1 indicate that the as-prepared PS spheres with a monodisperse character are suitable to be used as templates. PS@SiO_2 spheres were prepared by coating SiO_2 on those PS beads terminated in -NH_2 group. And the shell thickness was controlled by adjusting the concentration of TEOS. All of the reactions were carried out at the same ammonia concentration under constant stirring. The formation procedure of PS@SiO_2, air@SiO_2 and air@C@SiO_2 core-shell NPs are illustrated in Scheme 1. The measured diameter of PS, PS@SiO_2 nanospheres, corresponding reflection peaks and shell thickness are summarized in Table 1.

Fig. 1 shows the SEM images of PS@SiO_2 NPs with different sizes. The PS@SiO_2 NPs are monodisperse with uneven surface compared to the pure PS beads. And the surface roughness of

RSC Advances Accepted Manuscript

PS@SiO_2 confirms the formation of silica shell on PS beads. Moreover, free standing SiO_2 particles are absent in the production. For comparison, SEM images in Fig. S2 shows the SiO_2 coated PS and $NH_3 \cdot H_2O$ modified PS NPs, respectively. When pure PS beads are used as core material, immobilized SiO_2 and freestanding SiO_2 particles are coexisted in the production indicating that SiO_2 could hardly coated on negatively charged PS beads directly (Fig. S2a).When the negatively charged PS beads have been modified by $NH_3 \cdot H_2O$ before coating, the surface of PS beads are fully occupied by the immobilized SiO_2 particles and freestanding SiO_2 particles were absent in the production (Fig. S2b).

The shell thickness of SiO_2 is strongly depends on the concentrations of TEOS, and the shell thickness is increased with the concentration of TEOS. PS beads terminated with $-NH_2$ group could change their surfaces charge from negative into neutral (or slightly positive-charged) and silica sols could easily nucleated on the surface of each PS beads and eventually merge and grow into a thin shell characterized by uniform thickness.

FTIR spectra of the PS NPs and the ammonium treated PS are shown in Fig. 2a. The characteristic bands of PS could be observed in both of the samples: C-H stretch around 3000 cm^{-1}, aromatic C-C stretch around 1470 cm^{-1}, C-H out-of plane bend at 765 cm^{-1}, and aromatic C-C out-of-plane bend at 700 cm^{-1}. The characteristic absorption of the amino group at 3404 cm^{-1} indicates the existence of –NH2 in the ammonium treated sample.

1H NMR was also used to confirm the existence of $-NH_2$ on PS NPs. Fig. 2b shows the ^1H NMR spectra and the proton attached to the primary amine ($-NH_2$) is observed at 7.2 ppm.

Fig. S3 show the electrophoretic measurement results of pure PS beads and $-NH_2$ terminated PS beads and the colloidal stability were apparent from electrophoretic measurements. The decrease

RSC Advances Accepted Manuscript

in electrophoretic mobility from -0.6914 to -0.2941 *u*m·cm/Vs indicate the successful of -NH_2 group anchored on the surface of PS NPs. A change in the zeta potential of the particles is observed from approximately -33.3 mV for a bare PS surface to -14.17 mV. Thus, the -NH_2 is successfully anchor on the surface of PS NPs.

The measured zeta potentials for the PS, PS@SiO_2 NPs are approximately –33.3 mv and –31.48 mv, respectively. And the zeta potential is high enough for the suspension to keep stable for several hours. Fig. S4 shows the transmittance changes of the PS@SiO_2 solution over times. The PS@SiO_2 sample (Fig. S4a) appeared very stable over 26 hours and the transmittance has only a little change (Fig.S4b). Thus, the homogeneous PS@SiO_2 spheres could be utilized to fabricate three dimensional (3D) PCs.

Fig. 3 displays the SEM image of large-scale domains of PS@SiO_2 crystalline arrays with dimensions approximately 20 um. The crystalline arrays are ordered 3D hexagonal close-packed structures. And both of the six-fold symmetry and high degree of crystalline order are reflected in the FFT spot pattern (shown in the insert of Fig. 2).Where peaks up to third orders are clearly present although some defects still exist in the crystalline arrays. The formation of defects maybe resulted from the evaporating of water molecule and hydroxyl group on the surface of PS@SiO_2 spheres during self-assembly and thermal treatment process. [37]

3.2. Air@C@SiO_2 nanospheres

The TEM images of various core−shell particles prepared at different TEOS concentration are shown in Fig. 4. For example, the PS@SiO_2 spheres with the core size of 180 nm, 200 nm, 240 nm and 290 nm are coated on silica shells with thicknesses of 20 nm, 25 nm, 30 nm and 25 nm in different TEOS concentration, respectively. The particle size and shell thickness of the core−shell

RSC Advances Accepted Manuscript

particles after calcination are listed in Table S2 (supporting information).

Traditional way for fabricating PCs of hollow shells involves two steps: first, the formation of colloidal crystals of core−shell particles and followed with the removal of organic core by corrosion or calcination. In this study, air@C@SiO_2 core-shell spheres were obtained by calcining the PS@SiO_2 PCs at 500 ºC for 2 h in argon, PCs of PS@SiO_2 calcined at 500 ºC for 2 h in air has also been prepared for comparison. PS cores were burned away when calcined in air while part of the carbon still remained inside the shell as absorb layers when calcination was carried out in argon. Thereby, bi-layer core-shell nanospheres composed by a thin carbon layer exist in the interior of silica shell was generated.

EDS element mapping of air@C@SiO_2 NPs in Fig. 5 is utilized to show the space distribution of Si, O, and C elements. The intense Si and O signals throughout the shells suggest that the SiO_2 shell is homogeneous. The enhanced C signals in the internal edge of SiO_2 shell manifest that the carbon black is originated from PS NPs.

3.3. Optical properties of PS, PS@SiO_2 and hollow SiO_2 photonic crystals

The microscopic images of PCs structurally colored films and the corresponding reflective spectra are shown in Fig. 6. The peak positions shift to longer wavelength as the shell thickness increased and the shift trend of reflection spectra is agree very well with others work. [25] The changes in reflection peak positions are resulted from the variation of inter-planar spacing and effective refractive index. The Bragg law is given by Eq (1) [34, 46-47]:

$$m\lambda_{peak} = 2d_{hkl}\left[n^2_{eff} - \sin^2\theta\right]^{1/2} \quad (1)$$

Where m is the order of diffraction, λ_{peak} is the wavelength of the reflection peak, d_{hkl} is the inter-planar spacing between (h k l) planes, n_{eff} is the effective reflective index of the crystalline

RSC Advances Accepted Manuscript

lattice, θ is the light incident angle. Generally, the (1 1 1) planes of photonic crystals are oriented parallel to the surface of the glass substrate. In the spectra measurements, we suppose that the direction of incident light perpendicular to the (1 1 1) planes (θ = 0). In the FCC structure, the inter-planar spacing of $d_{1\,1\,1}$ is shown in Eq. (2):

$$d_{111} = \left(\frac{2}{3}\right)^{1/2} D_{sphere} \quad (2)$$

where D_{sphere} is the diameter of the sphere. For a close packed structure n_{eff} is given by Eq. (3):

$$n_{eff} = \left[n^2_{sphere} f + n^2_{air}(1-f)\right]^{1/2} \quad (3)$$

Where n_{sphere} and n_{air} are the refractive index of PS spheres and air, respectively; f is the volume fraction of spheres.

For the PS@SiO_2 spheres, n_{sphere} can be calculated by using Eq. (4)

$$n_{sphere} = n_{PS} \frac{V_{PS}}{V} + n_{SiO_2} \frac{V_{SiO_2}}{V} \quad (4)$$

where n_{PS} and n_{SiO2} are the refractive index of PS and SiO_2 spheres; V_{PS} and V_{SiO2} are the volumes of PS and SiO_2 spheres; V is the total volume of each component ($V = V_{PS} + V_{SiO2}$). We assume that $n_{SiO2} = 1.46$, $n_{PS} = 1.59$ and f = 0.74 for a closed-packed FCC structure. [17]

Thus, For PS NPs,

$$\lambda = 2.382 D_{sphere}$$

And for PS@SiO_2 PCs,

$$n_{ps@SiO2} = 1.46 + 0.13 \times (r/R)^3$$

The reflection peak positions of PCs assembled by PS and PS@SiO_2 NPs in Fig. 7 indicate that there are some discrepancies exist between the calculated and measured values. And the above-mentioned difference could be resolved by taking defects of the PCs into account. Fig. 3 shows that some defects still exist in the PCs although the ordered packing of the PCs is

RSC Advances Accepted Manuscript

characterized by hexagonal close-packed arrays. Thus, the volume of the sphere is partly replaced by the solvent or air and the effective refractive index of the PCs is lower than 0.74.

Fig. 8 shows the variation tendency of reflection peak positions for different PCs films. And the stop band of the hollow SiO_2 PCs have an obvious blue-shift due to the decrease of effective refractive index (n_{eff}) and particle size during calcination when compared with PCs assembled by PS and PS@SiO_2. In order to theoretically calculate the Bragg diffraction peak, the Eq. (4) should be modified by using Eq. (5):

$$n_{sphere} = n_{air}\frac{V_{air}}{V} + n_{SiO_2}\frac{V_{SiO_2}}{V} \quad (5)$$

Where n_{air} is the refractive index of air; V_{air} is the volumes of air; V is the total volume of each component ($V = V_{air} + V_{SiO2}$). We assume that $n_{air} = 1$ and $n_{SiO2} = 1.46$. [19]

3.4 Photonic crystal of air@C@SiO_2 with enhanced color saturation

When calcination process was carried out in air, the sample shows an extremely weak color appearance. However, the color saturation was significantly enhanced while calcination process was carried out at 500 ^{o}C in argon. Fig. 9 shows the images of colored films and PCs domains assembled by air@C@SiO_2 NPs. Because the absorb materials originated from the carbonization of PS make the multiple scattering of lights reduced considerably while the reflection intensity caused by coherent scattering only slightly decreased. In this way, the color saturation could be enhanced significantly without disturbing the PCs arrays. In addition, PCs calcined in air and argon have the same color appearance, indicating that the black material originated from PS just absorb the incoherent scattering light and no contribution to the structural colors. Interestingly, the colorful PCs samples in powder form still possess brilliant structural colors (shown in Fig. 10), which could be used as physical pigments.

RSC Advances Accepted Manuscript

Conclusion

PS@SiO_2 core-shell nanoparticles with shell thickness ranging from 20 to 30 nm by coating uniform shells of amorphous silica on polystyrene beads which terminated with -NH_2 groups have been prepared. And the particle sizes could be easily controlled by manipulating the hydrolysis and condensation of the TEOS precursor. 3D PCs of PS and PS@SiO_2 were fabricated via vertical deposition. The PS cores were burned away when calcination in air while part of the carbon still remained inside the shell when calcination at 500 ^oC in argon. And bi-layered nanopheres composed of a carbon black layer in the interior of the silica shell were generated. Most importantly, the visibility of this hollow SiO_2 PCs was significantly enhanced without disturbing the PCs arrays when calcination was carried out in argon. And the black materials originated from PS just absorb incoherent scattering light and no contribution to the color appearance. This method will be widely spread to improve the color saturation without disturbing the PCs. Moreover, hollow SiO_2 photonic crystal with high color saturation will enrich the application of core-shell NPs in many fields such as bionic colors, paintings, cosmetics, and photonic papers.

Acknowledgements

This work was supported by the National Natural Science Foundation of China (51472153, 51232008).

References

1. S. G. J. J D Joannopoulos, J N Winn, R D Meade, *Journal*, 2008.

2. O. Painter, R. Lee, A. Scherer, A. Yariv, J. O'brien, P. Dapkus and I. Kim, *Science*, 1999, **284**, 1819-1821.

3. H. Altug and J. Vučković, *Appl. Phys. Lett.*, 2005, **86**, 111102.

RSC Advances Accepted Manuscript

4. Y. H. Liu, X. Y. Hu, D. X. Zhang, B. Y. Cheng, D. Z. Zhang and Q. B. Meng, *Appl. Phys. Lett.*, 2005, **86**, 151102.

5. M. Scalora, J. P. Dowling, C. M. Bowden and M. J. Bloemer, *Phys. Rev. Lett.*, 1994, **73**, 1368.

6. H. T. Yang and P. Jiang, *Langmuir*, 2010, **26**, 13173-13182.

7. Q. S. Jiang, C. Li, S. G. Shi, D. G. Zhao, L. Xiong, H. L. Wei and L. Yi, *J. Non·Cryst. Solids*, 2012, **358**, 1611-1616.

8. S. K. Yang, W. P. Cai, L. C. Kong and Y. Lei, *Adv. Funct. Mater.*, 2010, **20**, 2527-2533.

9. S. K. Yang, M. I. Lapsley, B. Q. Cao, C. L. Zhao, Y. H. Zhao, Q. Z. Hao, B. Kiraly, J. Scott, W. Z. Li and L. Wang, *Adv. Funct. Mater.*, 2013, **23**, 720-730.

10. K. Yamashita, Y. Yoshioka, K. Higashisaka, K. Mimura, Y. Morishita, M. Nozaki, T. Yoshida, T. Ogura, H. Nabeshi and K. Nagano, *Nat. Nanotechno.*, 2011, **6**, 321-328.

11. Y. Takeoka, S. Yoshioka, A. Takano, S. Arai, K. Nueangnoraj, H. Nishihara, M. Teshima, Y. Ohtsuka and T. Seki, *Angew. Chem. Int. Ed.*, 2013, **52**, 7261-7265.

12. S. John, *Phys. Rev. Lett.*, 1987, **58**, 2486.

13. E. Yablonovitch, *Phys. Rev. Lett.*, 1987, **58**, 2059.

14. M. Srinivasarao, *Chem. Rev.*, 1999, **99**, 1935-1962.

15. Y. Gotoh, H. Suzuki, N. Kumano, T. Seki, K. Katagiri and Y. Takeoka, *New J. Chem.*, 2012, **36**, 2171-2175.

16. Y. Takeoka, M. Honda, T. Seki, M. Ishii and H. Nakamura, *ACS Appl. Mater. Interfaces*, 2009, **1**, 982-986.

17. V. L. Colvin, *MRS Bull.*, 2001, **26**, 637-641.

18. X. L. Xu and S. A. Asher, *JACS*, 2004, **126**, 7940-7945.

RSC Advances Accepted Manuscript

19. L. Wang and S. A. Asher, *Chem. Mater.*, 2009, **21**, 4608-4613.

20. H. Nakamura and M. Ishii, *J. Appl. Polym. Sci.*, 2007, **103**, 2364-2368.

21. Y. Lu, Y. D.Yin, Z.Y. Li and Y. N. Xia, *Nano Lett.*, 2002, **2**, 785-788.

22. F. Caruso, M. Spasova, V. Salgueiriño‐Maceira and L. Liz‐Marzán, *Adv. Mater.*, 2001, **13**, 1090-1094.

23. Y. N. Xia, B. Gates, Y. D. Yin and Y. Lu, *Adv. Mater.*, 2000, **12**, 693-713.

24. K. P. Velikov, A. Moroz and A. van Blaaderen, *Appl. Phys. Lett.*, 2002, **80**, 49-51.

25. Z. Y. Zhong, Y. D. Yin, B. Gates and Y. N. Xia, *Adv. Mater.*, 2000, **12**, 206-209.

26. A. Guerrero‐Martínez, J. Pérez‐Juste and L. M. Liz‐Marzán, *Adv. Mater.*, 2010, **22**, 1182-1195.

27. H. Zou, S. Wu and J. Shen, *Chem. Rev*, 2008, **108**, 3893-3957.

28. Y. J. Wong, L. Zhu, W. S. Teo, Y. W. Tan, Y. Yang, C. Wang and H. Chen, *JACS*, 2011, **133**, 11422-11425.

29. F. Mahtab, Y. Yu, J. W. Lam, J. Liu, B. Zhang, P. Lu, X. Zhang and B. Z. Tang, *Adv. Funct. Mater.*, 2011, **21**, 1733-1740.

30. L. H. Jing, C. H. Yang, R. R. Qiao, M. Niu, M. H. Du, D. Y. Wang and M. Y. Gao, *Chem. Mater.*, 2009, **22**, 420-427.

31. B. Tan and S. E. Rankin, *Langmuir*, 2005, **21**, 8180-8187.

32. W. G. Leng, M. Chen, S. X. Zhou and L. M. Wu, *Langmuir*, 2010, **26**, 14271-14275.

33. W. Stöber, A. Fink and E. Bohn, *J. Colloid Interface Sci.*, 1968, **26**, 62-69.

34. Y. Lu, J. McLellan and Y. Xia, *Langmuir*, 2004, **20**, 3464-3470.

35. T.-S. Deng and F. Marlow, *Chem. Mater.*, 2012, **24**, 536-542.

RSC Advances Accepted Manuscript

36. Q. S. Jiang, J. Zhong, X. Hu, F. F. Song, K. Ren, H. L. Wei, L. Yi, *Colloid. Surface A*, 2012, **415**: 202-208.

37. H. L. Li, W. T. Dong, H.-J. Bongard and F. Marlow, *J. Phys. Chem. B*, 2005, **109**, 9939-9945.

38. H. Míguez, F. Meseguer, C. López, Á. Blanco, J. S. Moya, J. Requena, A. Mifsud and V. Fornés, *Adv. Mater.*, 1998, **10**, 480-483.

39. Z. Z. Gu, H. Uetsuka, K. Takahashi, R. Nakajima, H. Onishi, A. Fujishima and O. Sato, *Angew. Chem. Int. Ed.*, 2003, **42**, 894-897.

40. S. Yoshioka and Y. Takeoka, *ChemPhysChem*, 2014, **15**, 2209-2215.

41. J. D. Forster, H. Noh, S. F. Liew, V. Saranathan, C. F. Schreck, L. Yang, J. G. Park, R. O. Prum, S. G. Mochrie and C. S. O'Hern, *Adv. Mater.*, 2010, **22**, 2939-2944.

42. W. T. Wang, B. T. Tang, W. Ma, J. Zhang, B. Z. Ju and S. F. Zhang, *JOSA A*, 2015, **32**, 1109-1117.

43. C. I. Aguirre, E. Reguera and A. Stein, *ACS Appl. Mater. Interfaces*, 2010, **2**, 3257-3262.

44. X. Du and J. H. He, *J. Appl. Polym. Sci.*, 2008, **108**, 1755-1760.

45. I. Tissot, J. Reymond, F. Lefebvre and E. Bourgeat-Lami, *Chem. Mater.*, 2002, **14**, 1325-1331.

46. Z. Chen, P. Zhan, Z. Wang, J. Zhang, W. Zhang, N. Ming, C. T. Chan and P. Sheng, *Adv. Mater.*, 2004, **16**, 417-422.

47. H. Nakamura, M. Ishii, A. Tsukigase, M. Harada and H. Nakano, *Langmuir*, 2006, **22**, 1268-1272.

Figure Captions:

Scheme 1. Particle formation, colloidal crystal self-assemble and calcination of PS@SiO_2 and air@C@SiO_2 PCs.

RSC Advances Accepted Manuscript

Figure 1. PS@SiO_2 spheres prepared by coating uniform amorphous silica on different PS NPs：a)220nm ±5; b)250nm ±5; c)300nm ±5; d)340nm ±5.

Figure 2. (a) Infrared spectra (FTIR) of PS NPs and the ammonium -treated NPs. (b) 1H NMR spectra of the –NH2 modified PS.

Figure 3. SEM images of large-scale domains of PS@SiO_2 crystalline arrays with hexagonal close-packed structures. The insert in Fig. 2: FFT spot pattern of a single crystal domain.

Figure4. the TEM images of various core−shell particles prepared at the same TEOS concentration. For example, the PS@SiO_2 spheres with the core size of 180 nm, 200 nm, 240 nm and 290nm were coated on silica shells with thicknesses of 20 nm, 25nm, 30nm and 25 nm were fabricated at the same TEOS concentration, respectively.

Figure 5. EDX element mapping of the identical NPs of air@C@SiO_2 and air@ SiO_2.

Figure 6. Microscopic image (reflective model：a1-a2: colloidal crystal film of PS180, PS@SiO_2 220 nm; b1-b2: PS200, PS@SiO_2 250nm; c1-c3: PS240, PS@SiO_2 260 nm, PS@SiO_2 300nm; d1-d3: PS290, PS@SiO_2 310nm, PS@SiO_2 340nm;A-D is the corresponding reflective spectra of PCs of PS and PS@SiO_2 spheres at normal incidence.

Figure 7. The calculated and experimental reflection peak positions of PS and PS@SiO_2 PCs. Exp and cal represent the experimental and calculate, respectively.

Figure 8. Tendency of reflection peak positions of photonic crystal films.

Figure9.The optical images of colored films and photonic crystal domains of air@C@SiO_2 nanospheres. A. air@C@SiO_2 220 nm; B. air@C@SiO_2 250 nm; C. air@C@SiO_2 300 nm; air@C@$SiO_2$340 nm. The core size from A-D is 180 nm, 200 nm, 240 nm; 290 nm, separately.

RSC Advances Accepted Manuscript

Figure10. Photonic crystal domains of PS@SiO_2 NPs calcination at different environment. A-D: Calcination under argon protection. A'-D': Calcination in air. A. PS@SiO_2 220 nm; B. PS@SiO_2 250 nm; C. PS@SiO_2 300 nm; PS@SiO_2 340 nm. The core size from A-D is 180 nm, 200 nm, 240 nm; 290 nm, respectively.

RSC Advances Accepted Manuscript

Scheme 1.

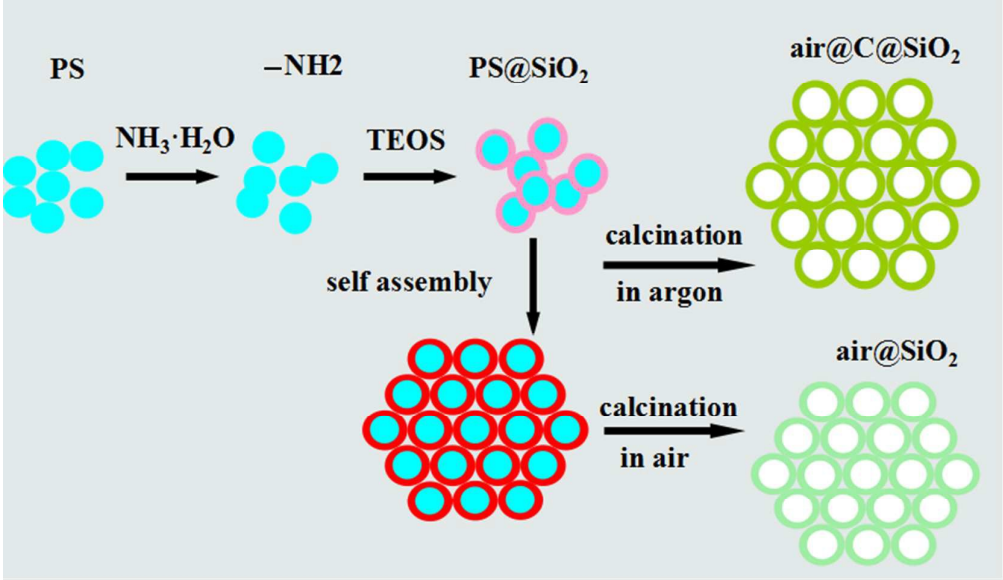

Scheme 1. Particle formation, colloidal crystal self-assemble and calcination of $PS@SiO_2$ and $air@C@SiO_2$ PCs.

RSC Advances Accepted Manuscript

Figure 1.

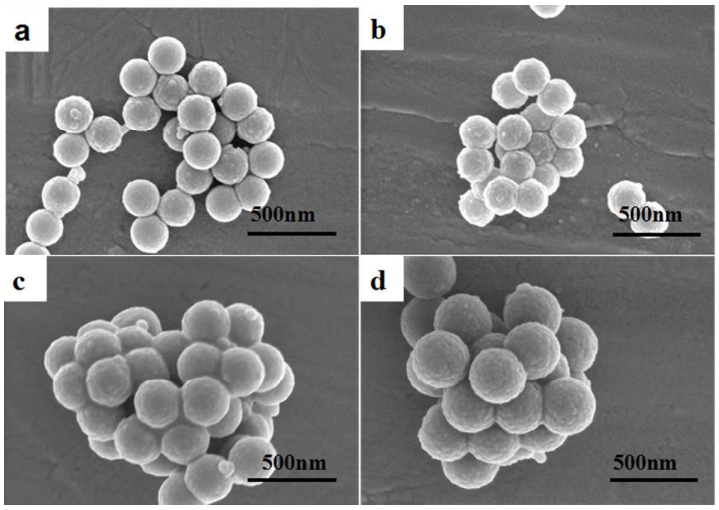

Figure 1. PS@SiO_2 spheres prepared by coating uniform amorphous silica on different PS NPs：

a)220nm ±5; b)250nm ±5; c)300nm ±5; d)340nm ±5.

RSC Advances Accepted Manuscript

Figure 2.

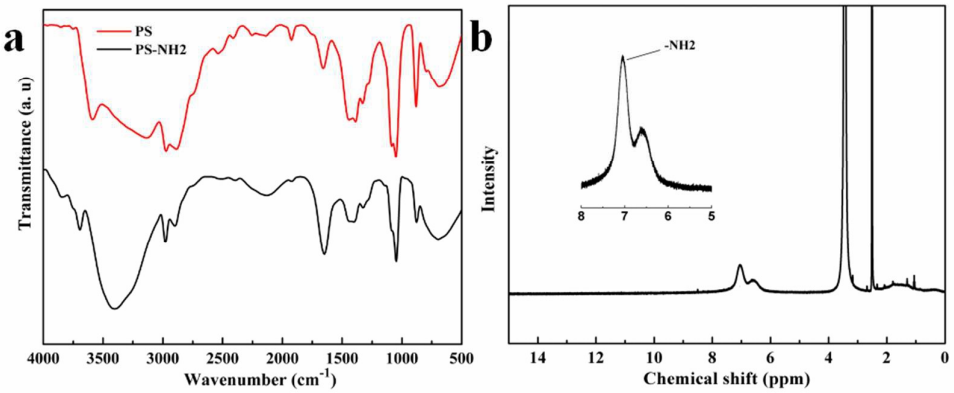

Fig. 2 (a) Infrared spectra (FTIR) of PS NPs and the ammonium -treated NPs. (b) 1H NMR spectra of the –NH2 modified PS.

RSC Advances Accepted Manuscript

Figure 3.

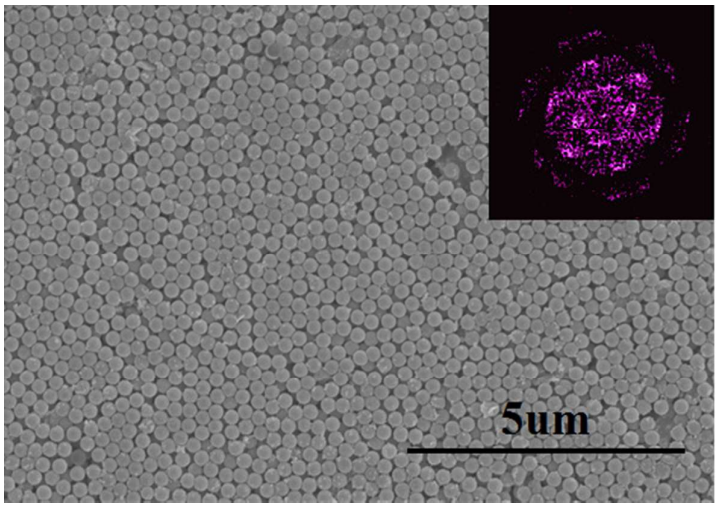

Figure 3. SEM images of large-scale domains of PS@SiO_2 crystalline arrays with hexagonal close-packed structures. The insert in Fig. 2: FFT spot pattern of a single crystal domain.

RSC Advances Accepted Manuscript

Figure4.

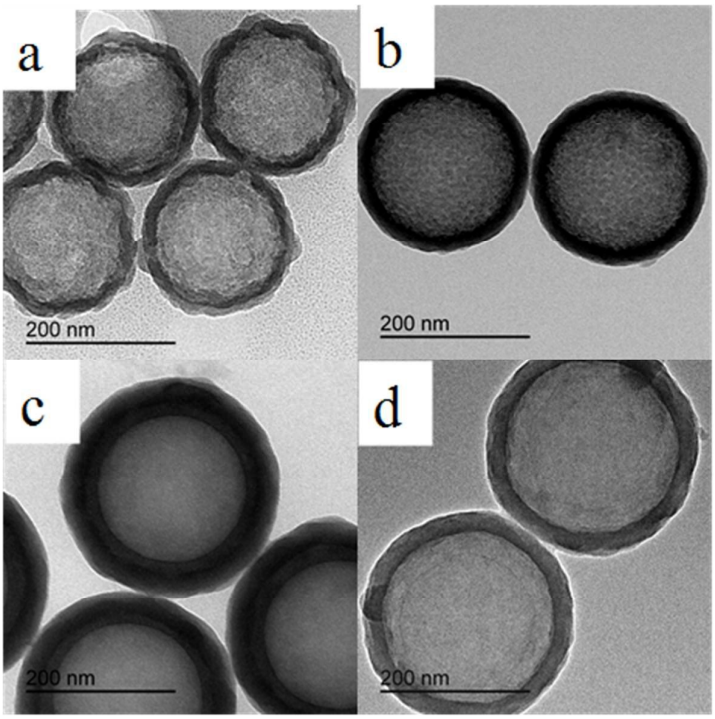

Figure4. the TEM images of various core−shell particles prepared at the same TEOS concentration.

For example, the PS@SiO_2 spheres with the core size of 180 nm, 200 nm, 240 nm and 290nm were coated on silica shells with thicknesses of 20 nm, 25nm, 30nm and 25 nm were fabricated at the same TEOS concentration, respectively.

RSC Advances Accepted Manuscript

Figure 5.

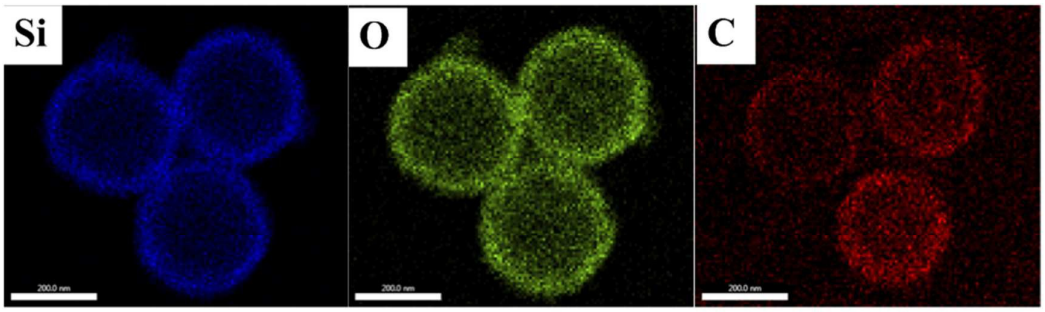

Figure 5. EDX element mapping of the identical NPs of air@C@SiO_2 and air@ SiO_2.

RSC Advances Accepted Manuscript

Figure 6

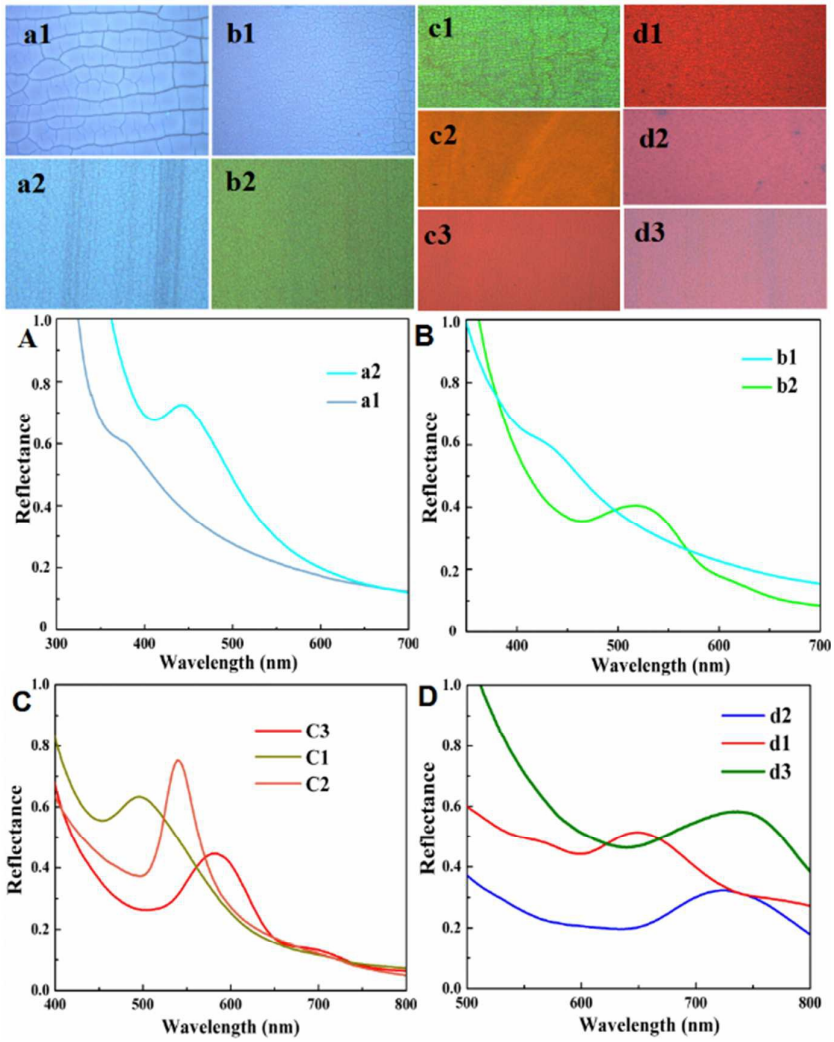

Figure 6. Microscopic image (reflective model：a1-a2: colloidal crystal film of PS180, PS@SiO_2 220 nm; b1-b2: PS200, PS@SiO_2 250nm; c1-c3: PS240, PS@SiO_2 260 nm, PS@SiO_2 300nm; d1-d3: PS290, PS@SiO_2 310nm, PS@SiO_2 340nm;A-D is the corresponding reflective spectra of PCs of PS and PS@SiO_2 spheres at normal incidence.

RSC Advances Accepted Manuscript

Figure. 7

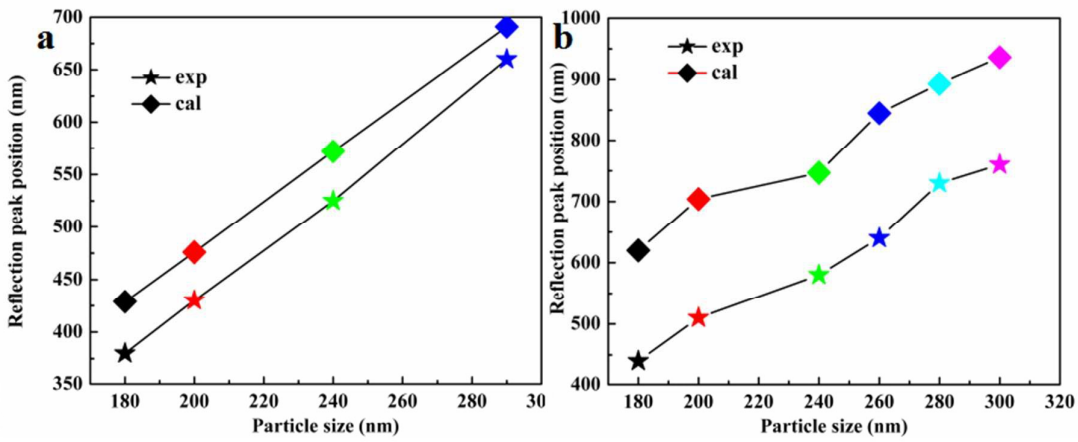

Fig.7 The calculated and experimental reflection peak positions of PS and PS@SiO_2 PCs. Exp and cal represent the experimental and calculate, respectively.

RSC Advances Accepted Manuscript

Figure 8.

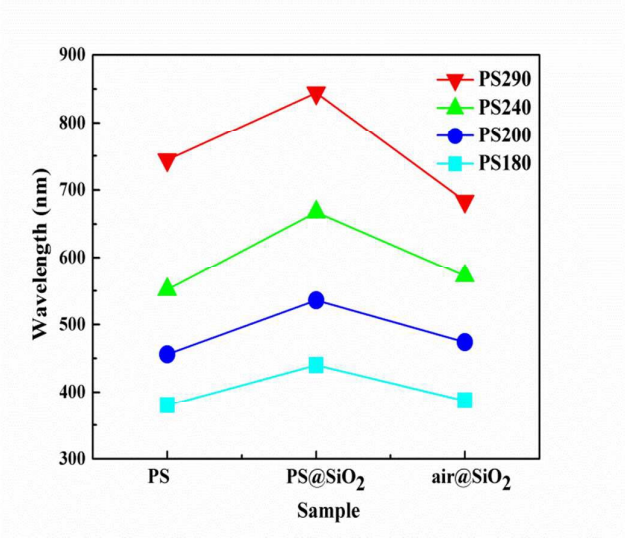

Figure 8. Tendency of reflection peak positions of photonic crystal films

RSC Advances Accepted Manuscript

Figure 9.

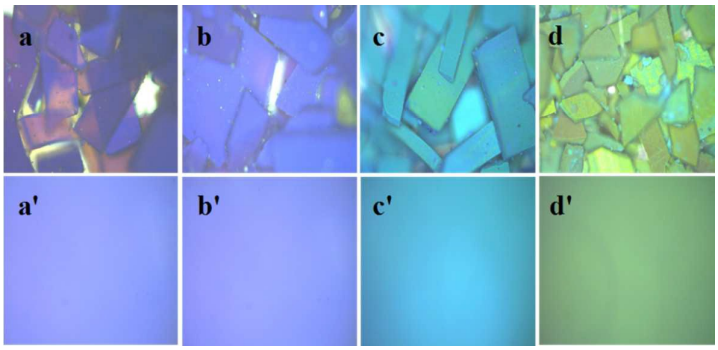

Figure9.The optical images of colored films and photonic crystal domains of air@C@SiO_2 nanospheres. A. air@C@SiO_2 220 nm; B. air@C@SiO_2 250 nm; C. air@C@SiO_2 300 nm; air@C@SiO_2 340 nm. The core size from A-D is 180 nm, 200 nm, 240 nm; 290 nm, separately.

RSC Advances Accepted Manuscript

Figure 10.

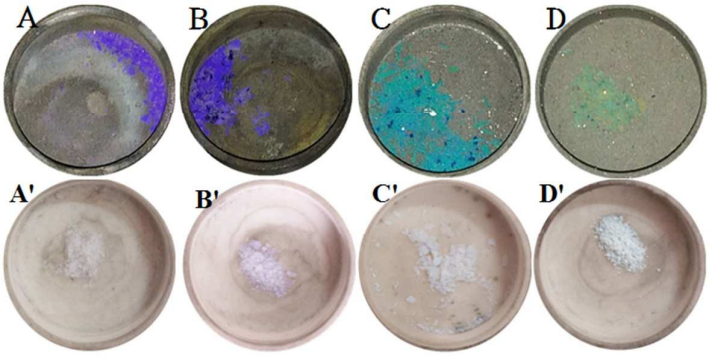

Figure 10. Photonic crystal domains of PS@SiO_2 NPs calcination at different environment. A-D: Calcination under argon protection. A'-D': Calcination in air. A. PS@SiO_2 220 nm; B. PS@SiO_2 250 nm; C. PS@SiO_2 300 nm; PS@SiO_2 340 nm. The core size from A-D is 180 nm, 200 nm, 240 nm; 290 nm, respectively.

RSC Advances Accepted Manuscript

Table 1.

Table 1. diameter and reflection peaks of PS and PS@SiO_2 photonic crystals and shell thickness of hollow SiO_2

sample	Core size (nm)	Ref peak (exp) (nm)	Ref peak (cal) (nm)	C_{TEOS} (uL)	$D_{PS@SiO2}$ (nm)	Ref peak(x) (nm)	Ref peak(cal) (nm)	Shell size (nm)
1	180±5	380	429	100	220±5	440	620	20
2	200±5	430	476	150	250±5	510	704	25
3	240±5	525	572	150	260±5	580	747	10
				200	300±5	640	845	30
4	290±5	660	691	150	310±5	730	893	10
				200	340±5	760	936	25

RSC Advances Accepted Manuscript